On Cyclic and Oscillatory Convection in a Simplified Box Model with Entrainment

Tomoki Tozuka
University of Tokyo, Japan

Abstract

Fluctuating ventilation effect in a simplified box model with three tubes is studied theoretically. A small basin is cooled from above and connected to an infinitely large isothermal basin with a layer of fresh water at the surface. A necessary condition for a new layer to form after a convection event is derived, and the model can reproduce 'cyclic convections' observed in past laboratory experiments. A parameterization for interfacial entrainment is formulated based on a potential energy budget. This introduces two new regimes to the model. One is an equilibrium state with the interface located in between the middle tube and the bottom tube with inflows at the top and bottom tube and an outflow at the middle tube. The other is an 'oscillatory ventilation' where the upper layer thickness does not grow monotonously, but oscillates. This regime is a result of balances between entrainment, surface cooling, and flow through the three tubes. Comparisons with laboratory experiments are made.

1 Introduction

The thermohaline circulation has been studied extensively due to its importance to global climate variation. The deep convection branch of the thermohaline circulation occurs in very confined regions[1],[2], and the Nordic Sea is one of the important sites. Since the salinity is very low in the surface layer of the Nordic Sea, the convection caused by the intense surface cooling cannot reach to a great depth without an increase in salinity. Excluding the dense overflow, the most probable candidate for a source of salinity increase seems to be the salty water below the surface[3]. In an attempt to understand this process, Whitehead[4] analyzed a simple box model both analytically and numerically. The model consisted of a small basin cooled from above and a large isothermal basin with a surface fresh water layer maintained at constant thickness. The two basins were connected to each other by three tubes at top, middle, and bottom. Using a relaxation boundary condition for the temperature, multiple equilibria were obtained. As an extension of this study, te Raa[5] performed laboratory experiments and showed that two flow regimes exist; one is a self-sustained oscillation and the other is a steady-state with deep convection. However, the mechanism for this oscillation remains unexplained theoretically. Also, an interfacial mixing process was not considered in the box model theory.

In this study, we expand earlier studies of oscillatory behavior in the simplified box model. The paper is organized as follows. In the next section, a description of a three-tube model and its behavior is presented. A necessary condition for the formation of a new layer after a convection event is derived. Also, a parameterization for the entrainment is formulated based on a discussion of potential energy budget. The theoretical model can then reproduce oscillations observed in the past laboratory experiments. In section 3, theoretical results are compared to laboratory experiment data. Conclusions are given in the final section.

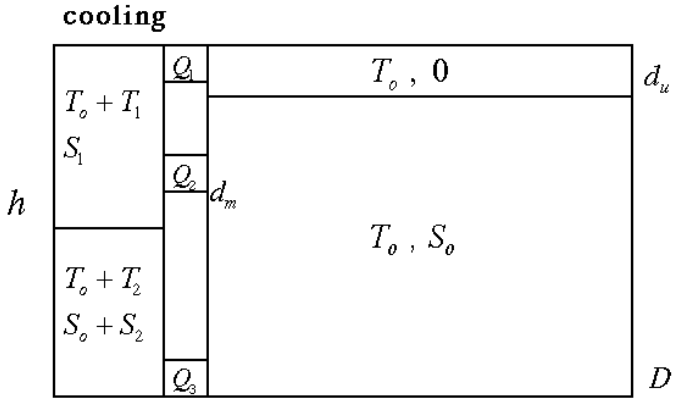

Figure 1: Schematic sketch of the three-tube model.

2 Three-tube Model

2.1 Formulation

Following Whitehead[4], a three-tube model is formulated here so that we can investigate the role played by the subsurface salty water. The importance of the middle tube may be further appreciated by comparing the result obtained here with two-tube model results presented in the Appendix.

A small basin, which represents a small region which contains a deep convection site, is cooled from above. This basin is connected to an infinitely large isothermal basin with three tubes, one at the surface, the second one at a depth of d_m, and the third one at the bottom. This differs from Whitehead[4], where the middle tube was placed at the depth of $D/2$. The depth of both basins is equal at D. A shallow fresh water layer of depth d_u with temperature T_o are maintained on top with temperature T_o and salinity S_o in the larger basin. The parameters in the large basin d_u, T_o, and S_o are kept fixed. In response to the surface cooling, the small basin contains a well-mixed surface layer of depth h, temperature $T_o + T_1$, and salinity S_1. The parameters in the small basin h, T_1, and S_1 can vary with time. A sketch of the box model is given in Fig.1.

We assume that a linear flow resistance in the tubes maintains a relation between the volume fluxes through the tubes Q_i and the pressure difference between two basins of the form

$$Q_i = C_i(p_{oi} - p_i) \text{ for } i = 1, 2, 3 \tag{1}$$

where we specify that

$$C_1 = \gamma C \ , \ C_2 = C_3 = C \tag{2}$$

are hydraulic resistances of tube i, and γ is a positive real number. Let η denote the fluid surface elevation of the small basin relative to the large basin. Then, from the hydrostatic relation, the pressure at tube i is given by

$$p_{o1} = 0 \tag{3}$$

$$p_{o2} = \rho_o g[d_u + (1 + \beta S_o)(d_m - d_u)] \tag{4}$$

$$p_{o3} = \rho_o g[d_u + (1 + \beta S_o)(D - d_u)] \tag{5}$$

in the large basin and

$$p_1 = \rho_o g \eta \tag{6}$$

$$p_2 = \left\{ \begin{array}{l} \rho_o g[\eta + (1 + \beta S_1 - \alpha T_1)h + (1 + \beta(S_o + S_2) - \alpha T_2)(d_m - h)] \text{ for } 0 < h \leq d_m \\ \\ \rho_o g[\eta + (1 + \beta S_1 - \alpha T_1)d_m] \text{ for } d_m \leq h \leq D \end{array} \right\} \tag{7}$$

$$p_3 = \rho_o g[\eta + (1 + \beta S - \alpha T)h + (1 + \beta(S_o + S_2) - \alpha T_2)(D - h)] \tag{8}$$

in the small basin. Here, the density is calculated using a linear equation of state and ρ_o is the density of fresh water at temperature T_o. The volume fluxes Q_i obey

$$Q_1 = -\gamma C \rho_o g \eta \tag{9}$$

$$Q_2 = \left\{ \begin{array}{l} C\rho_o g[-\eta - \beta S_o d_u + (-\beta S_2 + \alpha T_2)d_m \\ +(\beta(S_o + S_2 - S_1) + \alpha(T_1 - T_2))h] \text{ for } 0 < h \leq d_m \\ \\ C\rho_o g[-\eta - \beta S_o d_u + (\beta(S_o - S_1) + \alpha T_1)d_m] \text{ for } d_m \leq h \leq D \end{array} \right\} \tag{10}$$

$$Q_3 = C\rho_o g[-\eta - \beta S_o d_u + (-\beta S_2 + \alpha T_2)D + (\beta(S_o + S_2 - S_1) + \alpha(T_1 - T_2))h] \ . \tag{11}$$

Assuming that changes in the vertical acceleration with time are small, we obtain

$$\eta = \frac{1}{2 + \gamma}[-2\beta S_o d_u + 2(\beta(S_o + S_2 - S_1) + \alpha(T_1 - T_2))h + (-\beta S_2 + \alpha T_2)(D + d_m)] \tag{12}$$

for $0 < h \leq d_m$, and

$$\begin{aligned} \eta = \frac{1}{2 + \gamma}[&-2\beta S_o d_u + (\beta(S_o - S_1) + \alpha T_1)d_m + (-\beta S_2 + \alpha T_2)D \\ &+(\beta(S_o + S_2 - S_1) + \alpha(T_1 - T_2))h] \end{aligned} \tag{13}$$

for $d_m \leq h \leq D$. Substituting (12) into (9), (10), and (11), we obtain

$$\begin{aligned} Q_1 = -\frac{\gamma C \rho_o g \beta S_o D}{2 + \gamma}[&-\frac{2d_u}{D} + 2(1 + \frac{S_2}{S_o} - \frac{S_1}{S_o} + \frac{\alpha}{\beta S_o}(T_1 - T_2))\frac{h}{D} \\ &+(-\frac{S_2}{S_o} + \frac{\alpha T_2}{\beta S_o})(1 + \frac{d_m}{D})] \end{aligned} \tag{14}$$

$$Q_2 = \frac{C\rho_o g\beta S_o D}{2+\gamma}[-\gamma\frac{d_u}{D} + (-\frac{S_2}{S_o} + \frac{\alpha T_2}{\beta S_o})((1+\gamma)\frac{d_m}{D} - 1) \\ +\gamma(1 + \frac{S_2}{S_o} - \frac{S_1}{S_o} + \frac{\alpha}{\beta S_o}(T_1 - T_2))\frac{h}{D}] \tag{15}$$

$$Q_3 = \frac{C\rho_o g\beta S_o D}{2+\gamma}[-\gamma\frac{d_u}{D} + (-\frac{S_2}{S_o} + \frac{\alpha T_2}{\beta S_o})(1+\gamma - \frac{d_m}{D}) \\ +\gamma(1 + \frac{S_2}{S_o} - \frac{S_1}{S_o} + \frac{\alpha}{\beta S_o}(T_1 - T_2))\frac{h}{D}] \tag{16}$$

for $0 < h \leq d_m$, and substituting (13) into (9), (10), and (11), we obtain

$$Q_1 = -\frac{\gamma C\rho_o g\beta S_o D}{2+\gamma}[-\frac{2d_u}{D} + (\beta(1 - \frac{S_1}{S_o}) + \frac{\alpha T_1}{\beta S_o})\frac{d_m}{D} + (-\frac{S_2}{S_o} + \frac{\alpha T_2}{\beta S_o}) \\ +(1 + \frac{S_2}{S_o} - \frac{S_1}{S_o} + \frac{\alpha}{\beta S_o}(T_1 - T_2))\frac{h}{D}] \tag{17}$$

$$Q_2 = \frac{C\rho_o g\beta S_o D}{2+\gamma}[-\gamma\frac{d_u}{D} + (1 - \frac{S_1}{S_o} + \frac{\alpha T_1}{\beta S_o})(1+\gamma)\frac{d_m}{D} - (-\frac{S_2}{S_o} + \frac{\alpha T_2}{\beta S_o}) \\ -(1 + \frac{S_2}{S_o} - \frac{S_1}{S_o} + \frac{\alpha}{\beta S_o}(T_1 - T_2))\frac{h}{D}] \tag{18}$$

$$Q_3 = \frac{C\rho_o g\beta S_o D}{2+\gamma}[-\gamma\frac{d_u}{D} - (1 - \frac{S_1}{S_o} + \frac{\alpha T_1}{\beta S_o})\frac{d_m}{D} + (1+\gamma)(-\frac{S_2}{S_o} + \frac{\alpha T_2}{\beta S_o}) \\ +(1+\gamma)(1 + \frac{S_2}{S_o} - \frac{S_1}{S_o} + \frac{\alpha}{\beta S_o}(T_1 - T_2))\frac{h}{D}] \tag{19}$$

for $d_m \leq h \leq D$.

The upper layer mass conservation equation is

$$A\frac{dh}{dt} = Q_1 \tag{20}$$

for $0 < h \leq d_m$, and

$$A\frac{dh}{dt} = Q_1 + Q_2 \tag{21}$$

for $d_m \leq h \leq D$. The heat and salt balance equations are

$$Ah\frac{dT_1}{dt} = \frac{K_a}{\rho_o c_p}(T^* - T_1) - T_1 Q_1 \Gamma(+Q_1) \tag{22}$$

$$Ah\frac{dS_1}{dt} = -S_1 Q_1 \Gamma(+Q_1) \tag{23}$$

$$A(D-h)\frac{dT_2}{dt} = -T_2Q_2\Gamma(+Q_2) - T_2Q_3\Gamma(+Q_3) \tag{24}$$

$$A(D-h)\frac{dS_2}{dt} = -S_2Q_2\Gamma(+Q_2) - S_2Q_3\Gamma(+Q_3) \tag{25}$$

for $0 < h \leq d_m$, and

$$Ah\frac{dT_1}{dt} = \frac{K_a}{\rho_o c_p}(T^* - T_1) - T_1Q_1\Gamma(+Q_1) - T_1Q_2\Gamma(+Q_2) \tag{26}$$

$$Ah\frac{dS_1}{dt} = -S_1Q_1\Gamma(+Q_1) + (S_o - S_1)Q_2\Gamma(+Q_2) \tag{27}$$

$$A(D-h)\frac{dT_2}{dt} = -T_2Q_3\Gamma(+Q_3) \tag{28}$$

$$A(D-h)\frac{dS_2}{dt} = -S_2Q_3\Gamma(+Q_3) \tag{29}$$

for $d_m \leq h \leq D$. Here, we have taken that heat flux is proportional to $T^* - T_1$. This is called a restoring boundary condition for the temperature, and is also known as Haney boundary condition[6]. A zero salt-flux boundary condition is used.

When the density stratification in the small basin becomes unstable:

$$\rho(T_o + T_1, S_1) > \rho(T_o + T_2, S_o + S_2) \tag{30}$$

a convective adjustment occurs.

2.2 Parameterization of Entrainment

It is well known that entrainment plays an important role in upper ocean dynamics. In addition, te Raa[5] observed a strong interfacial entrainment in laboratory experiments. Thus, we here formulate an one-dimensional mixed layer model, which parameterizes the entrainment process at the interface, following Kraus and Turner[7] and Davis *et al.*[8]. We expect that an inclusion of entrainment should lead to more realistic representation of situations in the ocean and the laboratory experiment of te Raa[5]. The model results without the entrainment are provided in the Appendix.

The upper-layer potential energy is defined as

$$P = g\int_{-D}^{0}(z - z_o)\rho dz \tag{31}$$

where $z = z_o$ is a reference level, and $z = -D$ is a level below the mixed layer at which turbulent and radiative fluxes of heat is assumed to be negligible. The density conservation equation is

$$\frac{\partial \rho}{\partial t} + \frac{\partial}{\partial z}\overline{w'\rho'} = 0 \tag{32}$$

where $\overline{w'\rho'}$ is the vertical turbulent flux of mass. Here, advective terms have been neglected, because we cannot incorporate their effect in simple models such as the one considered in this study. Multiplying Eq.(32) by $g(z - z_o)$ and integrating it from $z = -D$ to $z = 0$, we obtain

$$\frac{\partial P}{\partial t} = g \int_{-D}^{0} \overline{w'\rho'} dz + \frac{\alpha g}{c_p} Q_o z_o \tag{33}$$

where

$$Q_o = \frac{c_p}{\alpha} \overline{w'\rho'}(0) = -c_p \rho \overline{w'T'}(0) \tag{34}$$

is the net downward heat flux at the surface. Note that the heat fluxes are assumed to vanish at $z = -D$.

From Tennekes and Lumley[9], the turbulent kinetic energy budget equation is

$$(\frac{\partial}{\partial t} + \mathbf{u} \cdot \nabla + w \frac{\partial}{\partial z}) \overline{e}_k = -g\overline{w'\rho'} - \rho \overline{\mathbf{u}w'} \cdot \frac{\partial}{\partial z}\mathbf{u} - \frac{\partial}{\partial z}\overline{w'(p' + e_k)} - \rho\epsilon \tag{35}$$

where

$$e_k = \frac{\rho}{2}(\mathbf{u} \cdot \mathbf{u} + w'^2) \ . \tag{36}$$

Here, the first term is the production of turbulent kinetic energy by the vertical buoyancy flux, the second term is the production of turbulent kinetic energy by shear, the third term is the vertical divergence of the turbulent flux of turbulent kinetic energy, and the final term is the viscous dissipation term. Again, the second term and the third term are beyond the framework of box model and are neglected. Also, based on the laboratory experiment, Deardorff *et al.*[10] showed that a fixed fraction m_c (=0.83) of potential energy gained by the surface cooling is dissipated. Thus, the potential energy equation (33) can be rewritten as

$$\frac{\partial P}{\partial t} = -m_c \frac{\alpha g D}{2c} Q_o + \frac{\alpha g}{c} Q_o z_o \ . \tag{37}$$

For the bulk mixed layer with thickness h, the potential energy equation is

$$\frac{gh}{2} \Delta\rho \frac{\partial h}{\partial t} = \frac{\alpha g}{c} [-\frac{h}{2} Q_o + \frac{h}{2} m_c Q_o] \ . \tag{38}$$

Therefore, the entrainment velocity in the three-tube model is parameterized by

$$w_e = -\frac{\alpha}{c_p \Delta\rho}(1 - m_c) Q_o \tag{39}$$

where $\Delta\rho$ is the density difference between the upper and lower layer. Since we are using the restoring boundary condition for heat, the entrainment velocity is

$$w_e = -\frac{\alpha(1 - m_c) K_a (T^* - T_1)}{c_p A \Delta\rho} \ . \tag{40}$$

Including the entrainment process, the upper layer mass conservation equation can be rewritten as

$$A\frac{dh}{dt} = Q_1 + Aw_e \tag{41}$$

for $0 < h \leq d_m$, and

$$A\frac{dh}{dt} = Q_1 + Q_2 + Aw_e \tag{42}$$

for $d_m \leq h \leq D$. The upper layer heat and salt balance equations are rewritten as

$$Ah\frac{dT_1}{dt} = \frac{K_a}{\rho_o c_p}(T^* - T_1) - T_1 Q_1 \Gamma(+Q_1) + A(T_2 - T_1)w_e \tag{43}$$

$$Ah\frac{dS_1}{dt} = -S_1 Q_1 \Gamma(+Q_1) + A(S_o + S_2 - S_1)w_e \tag{44}$$

for $0 < h \leq d_m$, and

$$Ah\frac{dT_1}{dt} = \frac{K_a}{\rho_o c_p}(T^* - T_1) - T_1 Q_1 \Gamma(+Q_1) - T_1 Q_2 \Gamma(+Q_2) + A(T_2 - T_1)w_e \tag{45}$$

$$Ah\frac{dS_1}{dt} = -S_1 Q_1 \Gamma(+Q_1) + (S_o - S_1) Q_2 \Gamma(+Q_2) + A(S_o + S_2 - S_1)w_e \tag{46}$$

for $d_m \leq h \leq D$.

2.3 Non-dimensionalized Equations

Using the transformations

$$\begin{gathered} \tilde{Q}_i = \frac{Q_i}{Q_{ss}} \ , \ \tilde{T}_i = \frac{\alpha T_i}{\beta S_o} \ , \ \tilde{d}_u = \frac{d_u}{D} \ , \ \tilde{d}_m = \frac{d_m}{D} \ , \\ \tilde{S}_i = \frac{S_i}{S_o} \ , \ \tilde{T^*} = \frac{\alpha T^*}{\beta S_o} \ , \ \tilde{t} = \frac{AD}{Q_{ss}} t \ , \ \tilde{K_a} = \frac{K_a}{\rho_o c_p Q_{ss}} \end{gathered} \tag{47}$$

where

$$Q_{ss} = \frac{\gamma C \rho_o g \beta S_o D}{2 + \gamma} \tag{48}$$

the model equations are non-dimensionalized as

$$\tilde{Q_1} = 2\tilde{d_u} - 2(1 + \tilde{S_2} - \tilde{S_1} + \tilde{T_1} - \tilde{T_2})\tilde{h} - (-\tilde{S_2} + \tilde{T_2})(1 + \tilde{d_m}) \tag{49}$$

$$\tilde{Q_2} = -\tilde{d_u} + (-\tilde{S_2} + \tilde{T_2})((\gamma^{-1} + 1)\tilde{d_m} - \gamma^{-1}) + (1 + \tilde{S_2} - \tilde{S_1} + \tilde{T_1} - \tilde{T_2})\tilde{h} \tag{50}$$

$$\tilde{Q_3} = -\tilde{d_u} + (-\tilde{S_2} + \tilde{T_2})(\gamma^{-1} + 1 - \gamma^{-1}\tilde{d_m}) + (1 + \tilde{S_2} - \tilde{S_1} + \tilde{T_1} - \tilde{T_2})\tilde{h} \tag{51}$$

$$\frac{d\tilde{h}}{d\tilde{t}} = \tilde{Q_1} + \tilde{w_e} \tag{52}$$

$$\tilde{h}\frac{d\tilde{T_1}}{d\tilde{t}} = \tilde{K_a}(\tilde{T^*} - \tilde{T_1}) - \tilde{T_1}\tilde{Q_1}\Gamma(+\tilde{Q_1}) + (\tilde{T_2} - \tilde{T_1})\tilde{w_e} \tag{53}$$

$$\tilde{h}\frac{d\tilde{S_1}}{d\tilde{t}} = -\tilde{S_1}\tilde{Q_1}\Gamma(+\tilde{Q_1}) + (1 + \tilde{S_2} - \tilde{S_1})\tilde{w_e} \tag{54}$$

$$(1 - \tilde{h})\frac{d\tilde{T_2}}{d\tilde{t}} = -\tilde{T_2}\tilde{Q_2}\Gamma(+\tilde{Q_2}) - \tilde{T_2}\tilde{Q_3}\Gamma(+\tilde{Q_3}) \tag{55}$$

$$(1 - \tilde{h})\frac{d\tilde{S_2}}{d\tilde{t}} = -\tilde{S_2}\tilde{Q_2}\Gamma(+\tilde{Q_2}) - \tilde{S_2}\tilde{Q_3}\Gamma(+\tilde{Q_3}) \tag{56}$$

for $0 < \tilde{h} \leq \tilde{d_m}$, and

$$\tilde{Q_1} = 2\tilde{d_u} - (1 - \tilde{S_1} + \tilde{T_1})\tilde{d_m} - (-\tilde{S_2} + \tilde{T_2}) - (1 + \tilde{S_2} - \tilde{S_1} + \tilde{T_1} - \tilde{T_2})\tilde{h} \tag{57}$$

$$\tilde{Q_2} = -\tilde{d_u} + (1 - \tilde{S_1} + \tilde{T_1})(1 + \gamma^{-1})\tilde{d_m} - \gamma^{-1}(-\tilde{S_2} + \tilde{T_2}) - \gamma^{-1}(1 + \tilde{S_2} - \tilde{S_1} + \tilde{T_1} - \tilde{T_2})\tilde{h} \tag{58}$$

$$\tilde{Q_3} = -\tilde{d_u} - \gamma^{-1}(1 - \tilde{S_1} + \tilde{T_1})\tilde{d_m} + (1 + \gamma^{-1})(-\tilde{S_2} + \tilde{T_2}) + (1 + \gamma^{-1})(1 + \tilde{S_2} - \tilde{S_1} + \tilde{T_1} - \tilde{T_2})\tilde{h} \tag{59}$$

$$\frac{d\tilde{h}}{d\tilde{t}} = \tilde{Q_1} + \tilde{Q_2} + \tilde{w_e} \tag{60}$$

$$\tilde{h}\frac{d\tilde{T_1}}{d\tilde{t}} = \tilde{K_a}(\tilde{T^*} - \tilde{T_1}) - \tilde{T_1}\tilde{Q_1}\Gamma(+\tilde{Q_1}) - \tilde{T_1}\tilde{Q_2}\Gamma(+\tilde{Q_2}) + (\tilde{T_2} - \tilde{T_1})\tilde{w_e} \tag{61}$$

$$\tilde{h}\frac{d\tilde{S_1}}{d\tilde{t}} = -\tilde{S_1}\tilde{Q_1}\Gamma(+\tilde{Q_1}) + (1 - \tilde{S_1})\tilde{Q_2}\Gamma(+\tilde{Q_2}) + (1 + \tilde{S_2} - \tilde{S_1})\tilde{w_e} \tag{62}$$

$$(1 - \tilde{h})\frac{d\tilde{T_2}}{d\tilde{t}} = -\tilde{T_2}\tilde{Q_3}\Gamma(+\tilde{Q_3}) \tag{63}$$

$$(1 - \tilde{h})\frac{d\tilde{S_2}}{d\tilde{t}} = -\tilde{S_2}\tilde{Q_3}\Gamma(+\tilde{Q_3}) \tag{64}$$

for $\tilde{d_m} \leq \tilde{h} \leq 1$. Here,

$$\tilde{w_e} = -(1 - m_c)\frac{\tilde{K_a}(\tilde{T^*} - \tilde{T_1})}{(1 + \tilde{S_2} - \tilde{T_2}) - (\tilde{S_1} - \tilde{T_1})} \ . \tag{65}$$

2.4 New Layer Formation

In laboratory experiments, it was observed that a new layer of low salinity water formed on top after a convective overturning (Whitehead, pers. comm.). In order to reproduce this phenomenon and resulting oscillations, we derive a necessary condition for this process to occur.

Fresh water flowing in from the top tube tries to form a new layer above the well-mixed thick layer of temperature $\tilde{T}_2$ and salinity $1 + \tilde{S}_2$ after a convective adjustment, or the interface reaching the bottom. Since the upper layer thickness is $\tilde{h} = 0$ then, the volume flux $\tilde{Q}_1$ is

$$\tilde{Q}_1 = \tilde{d}_u - \tilde{T}_2 + \tilde{S}_2 \ . \tag{66}$$

A new layer is formed on top with a thickness of

$$\tilde{h}_o = \tilde{Q}_1 \Delta\tilde{t} \tag{67}$$

after one time step $\Delta\tilde{t}$. However, the new layer is quickly cooled by the surface heat loss, $\tilde{K_a}\tilde{T}^*$, and becomes denser. From the heat balance equation, an increase in the density of the new layer after one time step is

$$\Delta\tilde{\rho}_1 = -\frac{\tilde{K_a}\tilde{T}^*\Delta\tilde{t}}{\tilde{Q}_1\Delta\tilde{t}} = -\frac{\tilde{K_a}\tilde{T}^*}{\tilde{Q}_1} \ . \tag{68}$$

To maintain static stability after the cooling,

$$\Delta\tilde{\rho}_1 = -\frac{\tilde{K_a}\tilde{T}^*}{\tilde{Q}_1} < 1 + (\tilde{S}_2 - \tilde{T}_2) \ . \tag{69}$$

Thus, the necessary condition for $\tilde{Q}_1$ to prevent convective overturning is

$$\tilde{Q}_1 > -\frac{\tilde{K_a}\tilde{T}^*}{1 + (\tilde{S}_2 - \tilde{T}_2)} \ . \tag{70}$$

Note that this condition is independent of the size of the time step. If this is not satisfied, the new layer becomes denser than the thick layer below, leading to another convective overturning. However, as the volume flux $\tilde{Q}_1$ progressively increases due to an increase in the density of the whole layer, the cooling of the thicker new layer decelerates. At some point, the above condition may be satisfied and the upper layer starts to grow again.

2.5 Steady-state Solutions

Numerous calculations were performed over varieties of parameter ranges and sensitivity of the model to dimensionless parameters were investigated. Calculations were initiated from $\tilde{T}_2 = \tilde{S}_2 = \tilde{S}_1 = \tilde{T}_1 = 0$ and $\tilde{h} = \tilde{d}_u$ with no flow at each tube.

Figure 2 shows the sensitivity of the model to the depth $\tilde{d_m}$. The inclusion of entrainment results in drastic changes in the equilibrium states. This can be compared with no

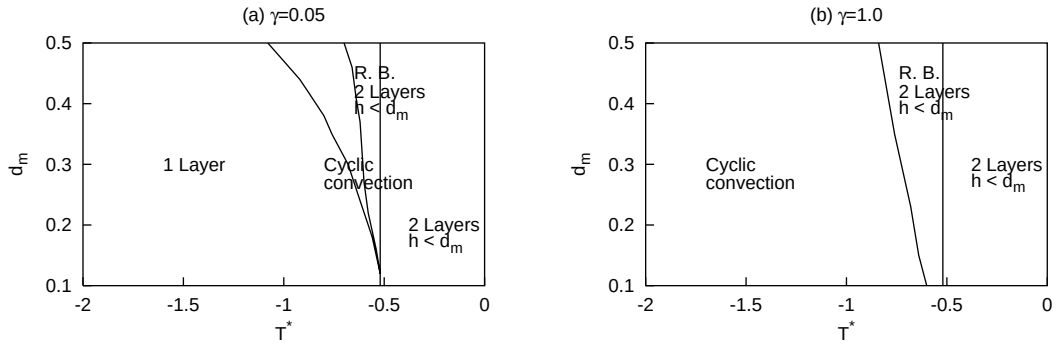

Figure 2: Regime diagrams for the three-tube model with entrainment at $\tilde{K_a} = 0.5$ and $\tilde{d_u} = 0.03$ for (a) $\gamma = 0.05$ and (b) $\gamma = 1.0$.

entrainment case illustrated in Fig. 11. When the cooling is weak, an equilibrium state with the interface above the middle-tube exists independent of γ (indicated by '2 Layers $h < d_m$'). The upper layer temperature becomes $\tilde{T}^*$ and all flow stops.

Since the entrainment leads to a faster upper layer deepening and faster increase in upper layer density due to the salinity, the upper layer either reaches the bottom or becomes statically unstable at much weaker cooling than without entrainment. The interface reaches the bottom with forcing temperature $\tilde{T}^*$ as high as -0.52 with entrainment, whereas it reaches the bottom only after $\tilde{T}^*$ is decreased below -1.06 without entrainment. For a small γ, an equilibrium state with only one layer emerges as the cooling is enhanced (indicated by '1 Layer'). For this regime, the upper layer either becomes statically unstable or reaches the bottom, but the volume flux $\tilde{Q}_1$ never accelerates enough to satisfy the necessary condition. The small basin has inflows through the top and middle tube, and outflow through the bottom tube. This corresponds to 'deep convection' state in te Raa[5].

Equilibrium states depend upon the depth of the middle tube for a large γ. When $\tilde{d_m}$ is deep, the interface reaches the bottom once, but the model reaches an equilibrium state with the interface above the middle tube (indicated by 'R.B. 2 Layer $h < d_m$'). On the other hand, an 'oscillatory ventilation' mode exists for shallower $\tilde{d_m}$. This regime is a result of subtle interplay between entrainment, surface cooling, and flow through the three tubes. The upper layer thickness does not grow monotonously, but oscillates in the 'oscillatory ventilation'. This is contrasted with 'cyclic convection', where the convection has a cyclic nature, but the upper layer grows monotonously. This regime appears as the cooling temperature is further decreased. They are discussed more in detail in the next section.

The model is also very sensitive to the upper layer depth of the large basin (Fig. 3). Another interesting equilibrium state exists for relatively deep $\tilde{d_u}$ with forcing temperature of $-0.58 < \tilde{T}^* < -0.46$ for large γ and $-0.76 < \tilde{T}^* < -0.46$ for small γ. The model reaches equilibrium with the interface located in between the middle tube and the bottom tube. Since the pressure difference at the bottom tube remains even after the model reaches the equilibrium, the inflow through the bottom tube persists. Thus, the water flows out from the small basin only through the middle tube and no deep water is formed in this

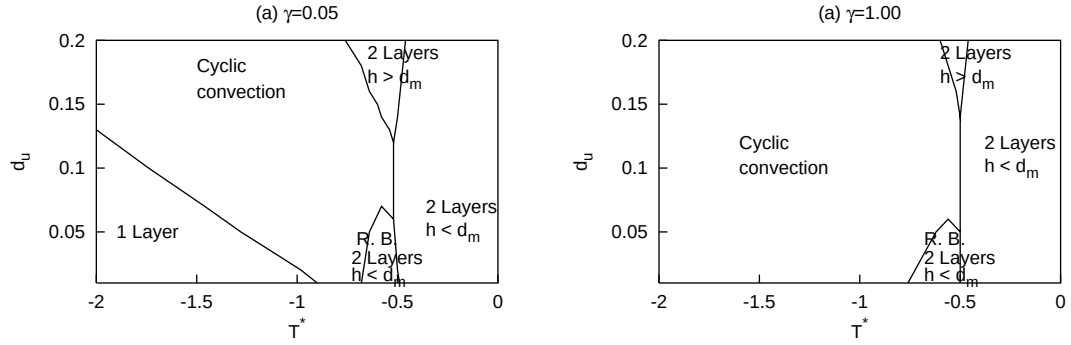

Figure 3: Regime diagrams for the three-tube model with entrainment at $\tilde{K_a} = 0.5$ and $\tilde{d}_m = 0.5$ for (a) $\gamma = 0.05$ and (b) $\gamma = 1.0$.

regime. A similar equilibrium state exists for three-tube model without entrainment, but the pressure difference at the bottom vanishes completely and the flow through the bottom tube stops ($\tilde{Q}_3 = 0$) when the equilibrium is reached. The time evolution of this regime is also discussed in the next section.

2.6 Time-dependent Solutions

For certain parameter range, very interesting oscillations are obtained (Fig.4), which do not exist in the model without entrainment (upper layer variables and thickness are set to zero in figures, when there is only one active layer after reaching the bottom or the convective adjustment). At $\tilde{t} = 40$, the interface reaches the bottom. As the volume flux $\tilde{Q}_1$ becomes large and satisfies the necessary condition (at $\tilde{t} = 41$), the upper layer starts to grow again. Although $\tilde{\rho}_1$ initially increases, it begins to decrease after $\tilde{Q}_2$ becomes negative, and the salinity source at the mid-depth is lost. Then, $\tilde{Q}_3$ (> 0) becomes larger than $\tilde{w_e}$, and the upper layer starts to become shallower. This is possible because the upper layer grows rapidly without increasing its density much, and the integrated mass above the bottom tube; the entrainment leads to faster deepening but only redistributes the mass within the small basin.

The inflow at the bottom tube ($\tilde{Q}_3 > 0$) causes both $\tilde{T}_2$ and $\tilde{S}_2$ to increase, and since the temperature increase is faster, $\tilde{\rho}_2$ decreases. This in turn makes the density difference $\tilde{\rho}_2 - \tilde{\rho}_1$ smaller, leading to an acceleration of the entrainment. The increased rate of entrainment results in an increase in $\tilde{S}_1$ and $\tilde{\rho}_1$, which leads to further decrease in the density difference and acceleration of the entrainment process. When $\tilde{w_e}$ becomes larger than $\tilde{Q}_3$ (at $\tilde{t} = 142$), the upper layer starts to grow again. Then, it reaches the bottom (at $\tilde{t} = 168$) and the whole cycle repeats itself.

A self-sustained 'cyclic convection' is also possible (Fig. 5). We start our description of this oscillation from $\tilde{t} = 4.3$, when the upper layer starts to grow. The upper layer temperature $\tilde{T}_1$ decreases rapidly due to the surface cooling, while the salinity $\tilde{S}_1$ increases slowly due to the entrainment. When the interface descends below the middle tube at $\tilde{t} = 5$, the warm and salty water flows into the upper layer of the small basin ($\tilde{Q}_2 > 0$), causing $\tilde{T}_1$

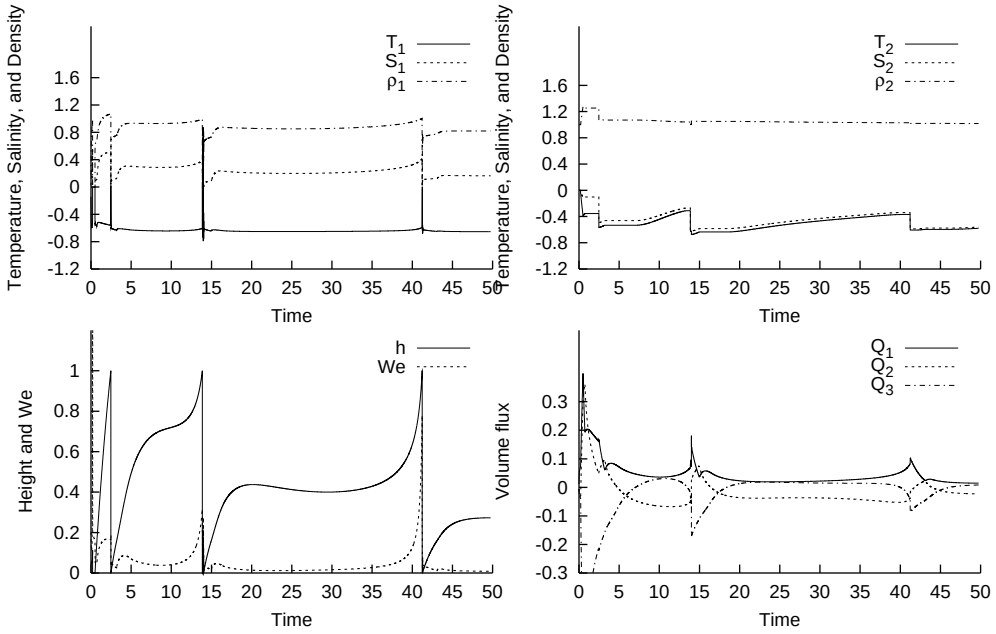

Figure 4: Time evolution of temperature, salinity, density, upper layer thickness, entrainment velocity, and flow rate at $\tilde{K_a} = 0.5$, $\tilde{d_u} = 0.03$, $\tilde{d_m} = 0.25$, $\tilde{T}^* = -0.54$, and $\gamma = 1.0$.

to initially increase and $\tilde{S}_1$ to increase steadily. At $\tilde{t} = 7.8$, the interface reaches the bottom and we now have one layer state in the small basin. Although the necessary condition for the new layer formation is not satisfied in the beginning, the density of the whole layer and the flow rate $\tilde{Q}_1$ gradually increase. Finally, the necessary condition for stable layer initiation is satisfied and the newly formed layer starts to grow from $\tilde{t} = 8.1$. The 'cyclic convection' is also seen in the three-tube model without entrainment and the two-tube mode (see Appendeces). However, the salinity plays no role in the 'cyclic convection' of the two-tube model.

Although it shows no oscillatory behavior, the equilibrium state with the interface in between the middle tube and the bottom tube shows very interesting features (Fig. 6), which cannot be obtained without the entrainment process. Until the interface reaches the middle tube (at $\tilde{t} = 6$), the outflow at the middle tube and the bottom tube have the same magnitude. After the interface descends below the middle tube, the outflow through the middle tube accelerates, while the flow at the bottom tube reverses (at $\tilde{t} = 8$). As the model approaches the equilibrium, the inflow through the bottom tube $\tilde{Q}_3$ and the entrainment velocity $\tilde{we}$ balance each other.

3 Comparison with Laboratory Experiments

The number of laboratory experiments is still limited, but we believe that it is worthwhile to make some comparison with the theoretical results obtained in the present study. The experimental set up is identical to the box model used in this study. The middle tube was placed at $\tilde{d_m} = 0.5$, and the surface fresh water layer of thickness $\tilde{d_u} = 0.05$ was maintained

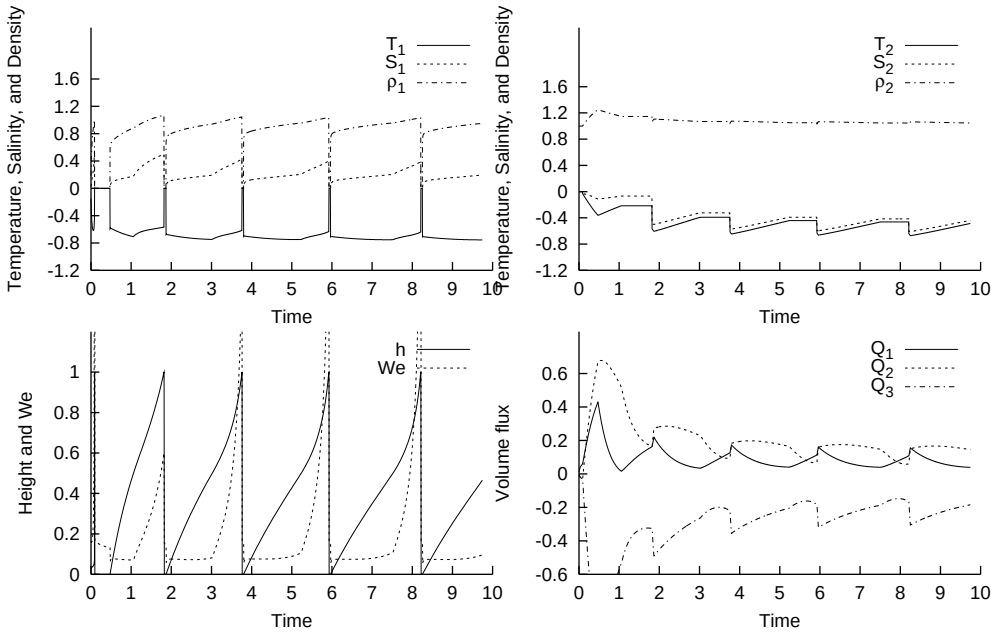

Figure 5: Time evolution of temperature, salinity, density, upper layer thickness, entrainment velocity, and flow rate at $\tilde{K_a} = 0.5$, $\tilde{d_u} = 0.03$, $\tilde{d_m} = 0.3$, $\tilde{T}^* = -1.0$, and $\gamma = 1.0$.

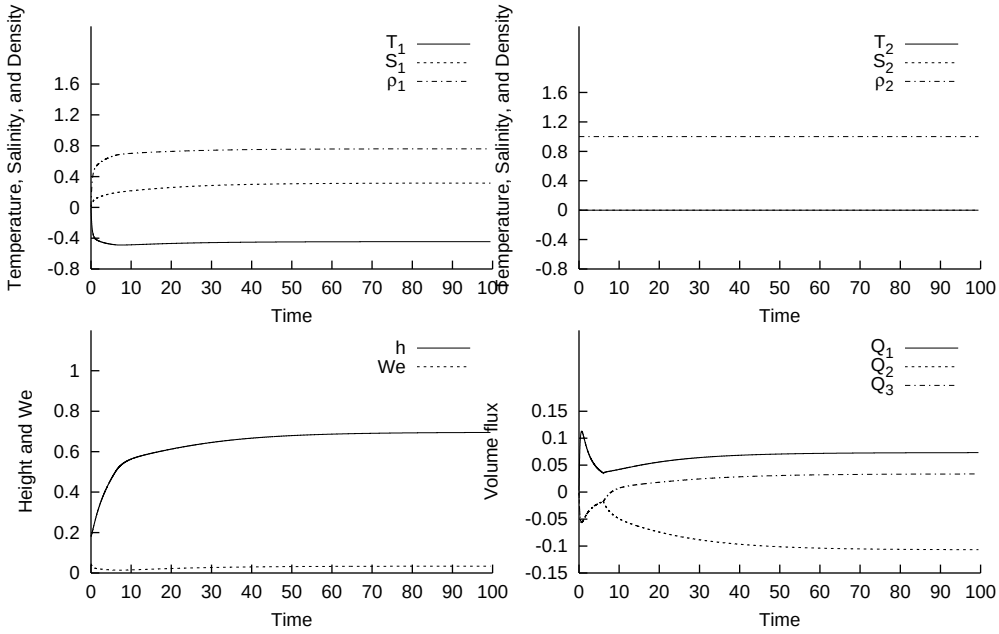

Figure 6: Time evolution of temperature, salinity, density, upper layer thickness, entrainment velocity, and flow rate at $\tilde{K_a} = 0.5$, $\tilde{d_u} = 0.18$, $\tilde{d_m} = 0.5$, $\tilde{T}^* = -0.54$, and $\gamma = 1.0$.

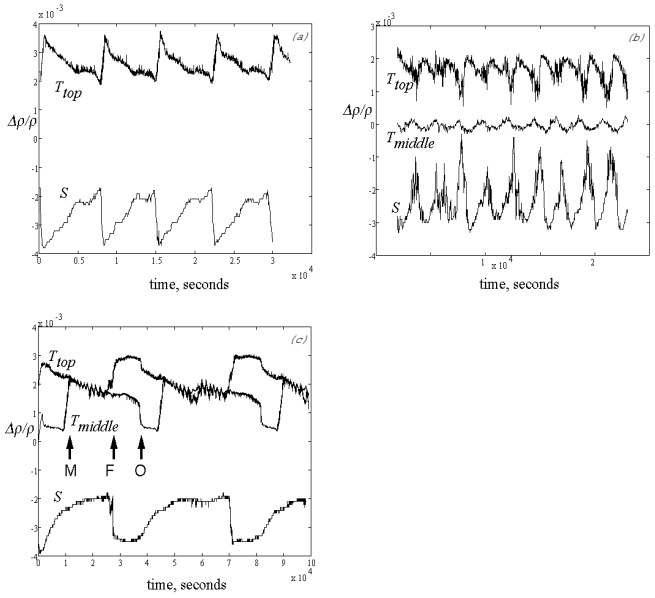

Figure 7: Time evolution of the temperature and salinity obtained in laboratory experiments with (a) $\tilde{T}^* = -22°C$, (b) $\tilde{T}^* = -30°C$, and $\tilde{T}^* = -18°C$ (provided by Whitehead).

in the large basin.

Figure 7 shows time evolution of the density contributions of temperature and salinity at different forcing temperature. All three experiments are similar to the behavior of 'cyclic convection'. For each cycle, the temperature at the top initially decreases due to the surface cooling. However, the temperature and salinity increase afterward due to the entrainment. When the density stratification becomes unstable, a convective overturning occurs and another cycle starts.

The experimental results further suggest that the period becomes shorter as the surface forcing is enhanced; the period is 40000 seconds for $\tilde{T}^* = -18°C$, 7500 seconds for $\tilde{T}^* = -22°C$, and 2200 seconds for $\tilde{T}^* = -30°C$. This is qualitatively consistent with our box model result (Fig. 8). The period becomes shorter, because the inflow through the top tube is larger and the entrainment velocity is faster when the surface forcing is enhanced.

Although an upside-down version of the three-tube model was used (heating is at the bottom and a layer of salty water is maintained at the bottom of the large basin) for practical reasons, experiments in te Raa[5] contain the same physics. Hence, more comparison are made with the present theory. In her experiments, the middle tube was also placed at $d_m = 0.5$, and the bottom salty water layer of thickness $d_u = 0.033$ was maintained in the large basin. From experiments, it was determined that $\tilde{K_a} = 1.2$ and $\gamma = 0.004$.

Our box model successfully explains some of the unexplained phenomena in the experiment. First, the mechanism for the shift in flow regime as the surface forcing is strengthened was unknown. In order to clarify this transition, we made a regime diagram of $\tilde{T}^*$ and γ (Fig. 9). We decided to vary γ in the regime diagram since γ seems to be the most uncertain value derived from the laboratory experiments. When γ is about 0.15, the present model successfully reproduces this shift at $\tilde{T}^* = -1.3$. The shift itself occurs, because it becomes

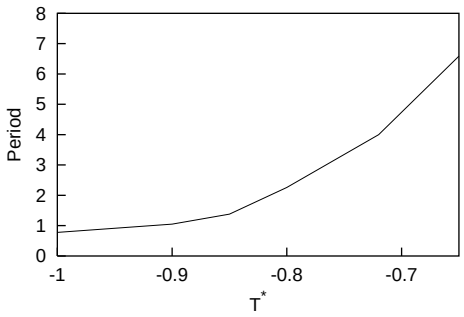

Figure 8: Period of 'cyclic convection' for $\tilde{K_a} = 0.5$ and $\tilde{K_a} = 1.0$, when $\tilde{d_u} = 0.05$ and $\tilde{d_m} = 0.5$.

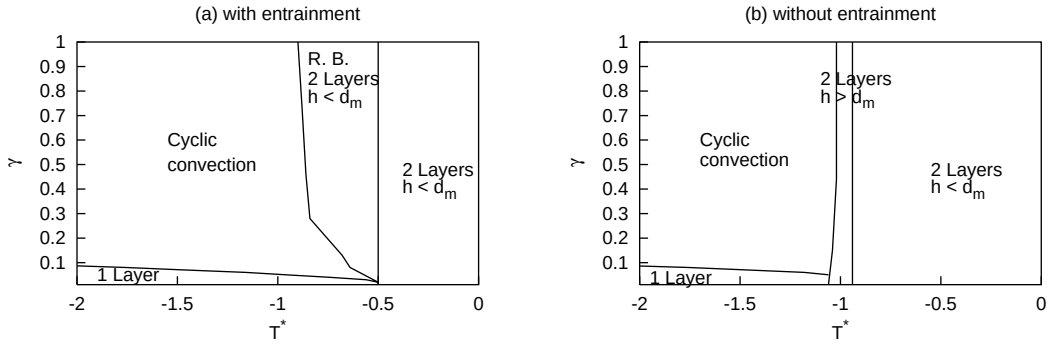

Figure 9: Regime diagrams for the three-tube model (a) with entrainment and (b) without entrainment at $\tilde{K_a} = 1.2$, $\tilde{d_u} = 0.033$, and $\tilde{d_m} = 0.5$.

more difficult to satisfy the necessary condition (70) as the surface forcing is enhanced. The volume flux $\tilde{Q}_1$ slowly increases with the strengthening forcing for small γ.

In addition, a reason for not being able to find the shallow convection state, or '2 Layers $h < d_m$' mode, is also clear from Fig. 9 . The shallow convection state exists only when $\tilde{T}^* > -0.50$ in the model with entrainment, whereas in the laboratory experiments of te Raa[5], $|\tilde{T}^*|$ was set between 0.8 and 1.7. If the entrainment is excluded from the box model, the existence of the shallow convection state is predicted in this forcing temperature range. Therefore, this gives an additional evidence that the entrainment is a crutial process here.

However, the period of oscillation in laboratory experiments, especially when the cooling is weak, is much longer in the experiments than in the box model theory. Also, the value of γ suggested from this study is much larger than the experimentally determined value of te Raa[5]. One possible reason for these inconsistencies is the linear flow relation we used in our box model; it may not correctly explain the flow through the three tubes in the laboratory experiments. Although the linear equation of state is used in this study, nonlinearity certainly becomes important as the temperature and salinity varies over a large range. Also, the double diffusive processes may play an important role, since the small basin is in the 'diffusive-layering' regime (cold and fresh water over warm and salty water).

4 Conclusions

We have found two distinct modes for the oscillatory behaviors of the simplified three-tube box model. Two new processes are included in the box model in the present study comapared with the past studies[4],[5].

First, the necessary condition for a new layer formation has been found. It applies after the convective adjustment occurs or the interface reaches the bottom. This allows the model to have 'cyclic convection'. Then, the entrainment process is parameterized, where a fixed percentage of potential energy input by the surface cooling is used to entrain water from the lower layer. This introduces two new equilibrium states to the model. One is the equilibrium state with the interface located in between the middle tube and the bottom tube. This has inflows at the top and bottom tube and an outflow at the middle tube. The other is an 'oscillatory' mode where the upper layer thickness does not grow monotonically, but oscillates. This regime is a result of subtle interplay between entrainment, surface cooling, and flow through the three tubes.

The current result may represent some aspects of the thermohaline circulation in the real ocean. As suggested by Fig. 3, a thickening in the surface fresh water layer outside the deep convection site may shut down the deep water formation without changing the heat flux (for small γ at about $-0.7 < \tilde{T}^* < -0.5$). For thick fresh water layer, a '2 Layers $h > d_m$' mode with inflows at the top and bottom tube and an outflow at the middle tube exists. On the other hand, we have a '1 Layer' mode with inflows at the top and middle tube and an outflow at the bottom tube for thin fresh water layer. This feature is also simulated in the past coupled GCM studies[11]. When freshwater was released to the North Atlantic Ocean (between $50°N$ and $70°N$), the thermohaline circulation weakened and became shallower, allowing deep inflow of Antarctic bottom water.

Although the box model presented in this paper is very simple, this study suggests the

important roles played by the freshwater layer above the halocline and salty water below it. Also, it was shown that it is important to take entrainment process into account even in simple box models. Future studies should shed light on the role played by the double diffusive process and nonlinearity in equation of state.

Acknowledgements

The author is very grateful to the supervisor, Jack Whitehead for his guidance of the whole summer project and his kindness in providing his laboratory experiment data. The author would like to express his sincere thanks to Claes Rooth for many fruitful discussions and valuable suggestions during the course of this study. Discussions with Joe Keller and Takamitsu Ito were both very helpful. Finally, I would like to thank all the fellows and GFD staffs for the great summer.

References

[1] H. Stommel, "On the smallness of sinking regions in the ocean," Proc. Nat. Aca. Sci. **48**, 766 (1962).

[2] J. A. Whitehead, "Thermohaline ocean processes and models," Ann. Rev. Fluid Mech. **27**, 89 (1995).

[3] Lab Sea Group, "The Labrador Sea deep convection experiment," Bull. Am. Met. Soc. **10**, 2033 (1998).

[4] J. A. Whitehead, "Stratified convection with multiple states," Ocean Modelling **2**, 109 (2000).

[5] L. te Raa, "Convective oscillations in a laboratory model," GFD Fellow Report **43**, 237 (2001).

[6] R. Haney, "Surface thermal condition for ocean circulation models," J. Phys. Oceanogr. **1**, 241 (1971).

[7] E. B. Kraus and J. S. Turner, "A one-dimensional model of the seasonal thermocline: II, The general theory and its consequences," Tellus **19**, 98 (1967).

[8] R. E. Davis, R. deSzoeke, and P. Niiler, "Variability in the upper ocean during MILE. Part II: Modeling the mixed layer response," Deep-Sea Res. **28**, 1453 (1981).

[9] H. Tennekes and J. L. Lumley, *A first course in turbulence* (M.I.T. Press, Cambridge, Massachusetts, 1972).

[10] J. W. Deardorff, G. E. Willis, and D. K. Lilly, "Laboratory investigation of non-steady penetrative convection," J. Fluid Mech. **35**, 7 (1969).

[11] S. Manabe and R. J. Stouffer, "Simulation of abrupt climate change induced by freshwater input to the north atlantic ocean," Nature **378**, 165 (1995).

Appendix A: Two-tube Model without Entrainment

Formulation

In this Appendix, a two-tube model is constructed by removing the middle tube. By comparing reslts obtained here with results in section 2, the importance of the middle tube will become more clear. Since we want to concentrate on the role played by the middle tube, the entraninment process is omitted from the two-tube model.

Using same assumptions, the volume fluxes are

$$Q_1 = -Q_2 = -\frac{\gamma C \rho_o g D}{\gamma + 1}[(\beta(S_o + S_2 - S_1) + \alpha(T_1 - T_2))\frac{h}{D} - \beta S_o \frac{d_u}{D} + (\alpha T_2 - \beta S_2)] \quad (71)$$

the upper layer mass conservation equation is

$$A\frac{dh}{dt} = Q_1 \quad (72)$$

and the heat and salt balance equations are

$$Ah\frac{dT_1}{dt} = \frac{K_a}{\rho_o c_p}(T^* - T_1) - T_1 Q_1 \Gamma(+Q_1) \quad (73)$$

$$Ah\frac{dS_1}{dt} = -S_1 Q_1 \Gamma(+Q_1) \quad (74)$$

$$A(D-h)\frac{dT_2}{dt} = -T_2 Q_2 \Gamma(+Q_2) \quad (75)$$

$$A(D-h)\frac{dS_2}{dt} = -S_2 Q_2 \Gamma(+Q_2)\ . \quad (76)$$

Using the following transformations

$$\tilde{Q}_i = \frac{Q_i}{Q_s}\ ,\ \tilde{T}_i = \frac{\alpha T_i}{\beta S_o}\ ,\ \tilde{d}_u = \frac{d_u}{D}\ ,\ \tilde{S}_i = \frac{S_i}{S_o}\ ,\ \tilde{T^*} = \frac{\alpha T^*}{\beta S_o}\ ,\ \tilde{t} = \frac{AD}{Q_s}t\ ,\ \tilde{K_a} = \frac{K_a}{\rho_o c_p Q_s} \quad (77)$$

where

$$Q_s = \frac{\gamma C \rho_o g \beta S_o D}{\gamma + 1} \quad (78)$$

the nondimensionalized equations are

$$\tilde{Q_1} = -\tilde{Q_2} = -[(1 + \tilde{S_2} - \tilde{S_1} + \tilde{T_1} - \tilde{T_2})\tilde{h} - \tilde{d_u} + (\tilde{T_2} - \tilde{S_2})] \quad (79)$$

$$\frac{d\tilde{h}}{d\tilde{t}} = \tilde{Q}_1 \tag{80}$$

$$\tilde{h}\frac{d\tilde{T}_1}{d\tilde{t}} = \tilde{K_a}(\tilde{T}^* - \tilde{T}_1) - \tilde{T}_1\tilde{Q}_1\Gamma(+\tilde{Q}_1) \tag{81}$$

$$\tilde{h}\frac{d\tilde{S}_1}{d\tilde{t}} = -\tilde{S}_1\tilde{Q}_1\Gamma(+\tilde{Q}_1) \tag{82}$$

$$(1-\tilde{h})\frac{d\tilde{T}_2}{d\tilde{t}} = -\tilde{T}_2\tilde{Q}_2\Gamma(+\tilde{Q}_2) \tag{83}$$

$$(1-\tilde{h})\frac{d\tilde{S}_2}{d\tilde{t}} = -\tilde{S}_2\tilde{Q}_2\Gamma(+\tilde{Q}_2)\ . \tag{84}$$

Thus, we have three dimensionless parameters for this simple model.

The necessary condition for a new layer formation is

$$\tilde{Q}_1 > -\frac{\tilde{K_a}\tilde{T}^*}{1+(\tilde{S}_2 - \tilde{T}_2)}\ . \tag{85}$$

However, there is an upper bound for the volume flux $\tilde{Q}_1$, which depends on the value of $\tilde{T}^*$ and $\tilde{d}_u$:

$$\tilde{Q}_1 < \tilde{d}_u - \tilde{T}^* \tag{86}$$

or

$$\tilde{Q}_1 < \tilde{d}_u - \tilde{T}^* - 1 \tag{87}$$

in case the small basin loses all of its salinity. This is possible when the upper layer reaches the bottom or after an infinite number of convective adjustments takes place. Hence, the new layer cannot form when

$$\tilde{d}_u - \tilde{T}^* < -\frac{\tilde{K_a}\tilde{T}^*}{1-\tilde{T}^* + \tilde{S}_2} \tag{88}$$

or

$$\tilde{d}_u - \tilde{T}^* - 1 < \tilde{K_a} \tag{89}$$

for no salinity.

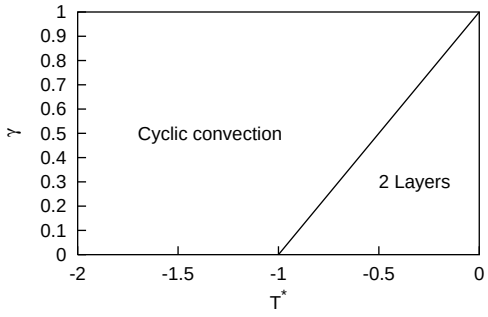

Figure 10: Regime diagrams for the the two-tube model with $\tilde{K}_a = 0.5$.

Steady-state Solutions

Equilibrium states of the model is discussed for progressively stronger cooling. When the cooling is weak, the model reaches equilibrium before the interface reaches the bottom. The upper layer temperature $\tilde{T}_1$ is quickly cooled and becomes $\tilde{T}^*$. The volume flux Q_1 and Q_2 become zero and the equilibrium depth of the upper layer is

$$\tilde{h}_{eq} = \frac{\tilde{d}_u}{\tilde{T}^* + 1} \ . \tag{90}$$

Since there is no interfacial mixing in this model, we have assumed that $\tilde{T}_2 = \tilde{S}_2 = \tilde{S}_1 = 0$.

In order to reach equilibrium before reaching the bottom ($\tilde{h}_{eq} < 1$),

$$\tilde{T^*}_c + 1 > \tilde{d}_u \tag{91}$$

For the forcing temperature below $\tilde{T^*}_c$, the interface reaches the bottom before reaching the equilibrium state. However, if the cooling is not strong enough to strengthen the flow to satisfy necessary condition, it is not possible to form a stable new layer. Now, we obtain a new equilibrium state with one fresh layer of temperature $\tilde{T}^*$, and the volume flux as predicted from Eq.(87). Finally, a third 'cyclic convection' regime can exist as the forcing temperature is decreased further. The above mentioned three regimes in the two-tube model can be summarized by Fig. 10.

Appendix B: Three-tube Model without Entrainment

Equilibrium states with different cooling temperature are investigated using different values of middle-tube depth $\tilde{d}_m$ (Fig.11). Equilibrium states have no γ-dependence at forcing temperature $\tilde{T}^*$ below -1.06. At weak cooling ($\tilde{T}^* < -0.72$), the model has an equilibrium state with the interface above the middle tube, but when the cooling is enhanced, the model reaches an equilibrium state with the interface between the middle tube and the bottom tube. For small γ, an equilibrium state with 1 layer emerges, when cooling is further

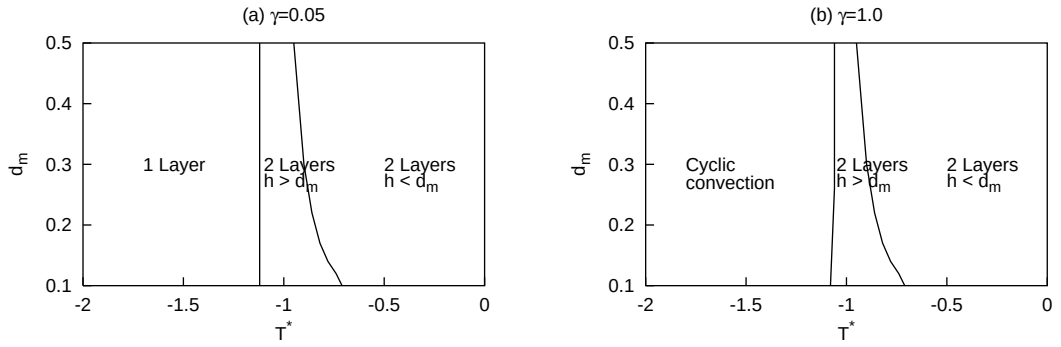

Figure 11: Regime diagrams for the three-tube model without entrainment at $\tilde{K_a} = 0.5$ and $\tilde{d_u} = 0.03$ for (a) $\gamma = 0.05$ and (b) $\gamma = 1.0$.

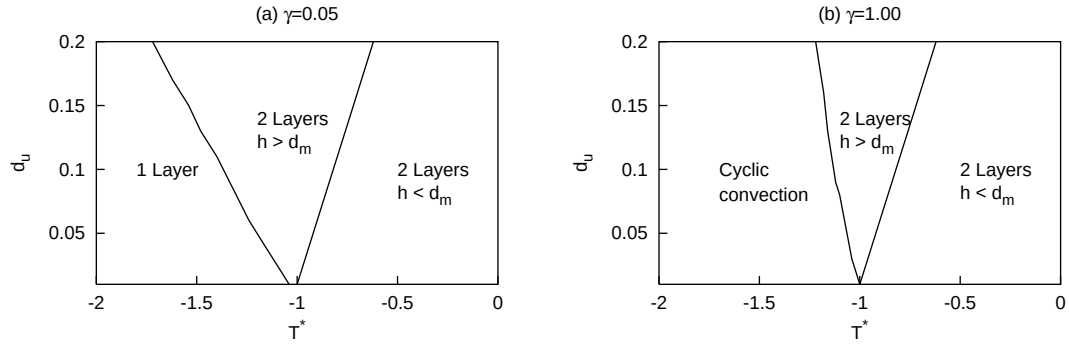

Figure 12: Regime diagrams for the three-tube model without entrainment at $\tilde{K_a} = 0.5$ and $\tilde{d_m} = 0.5$ for (a) $\gamma = 0.05$ and (b) $\gamma = 1.0$.

enhanced. On the other hand, 'cyclic convection' regime appears for large γ; with larger γ values, the volume flux at the top tube becomes larger, so that it is easier to satisfy the necessary condition (70).

Similarly, three-tube model is sensitive to the fresh water layer thickness of the large basin (Fig. 12). Compared with shallow $\tilde{d_u}$, the interface reaches the middle tube at warmer $\tilde{T}^*$, but the equilibrium states of 'cyclic convection' or '1 Layer' emerges at colder $\tilde{T}^*$ for deeper $\tilde{d_u}$.